On Convertibility From Antenna to Sensor Brightness Temperature for ATMS

Fuzhong Weng, Hu Yang, and Xiaolei Zou

***Abstract*—The Advanced Technology Microwave Sounder (ATMS) onboard the Suomi National Polar-orbiting Partnership (NPP) satellite is a total power radiometer and scans across the track within a range of $\pm 52.77^\circ$ from nadir. It has 22 channels and measures the microwave radiation at either quasi-vertical or quasi-horizontal polarization from the Earth's atmosphere. Without simultaneous measurements at both polarizations at the same frequency, the conversion from ATMS antenna temperature to sensor brightness temperature becomes nonunique if the antenna subsystem has a significant spillover from cross-polarization. In addition, the antenna temperature could be contributed from both the near- and far-field radiation through the sidelobes of the ATMS antenna subsystem. An analysis of the ATMS antenna gain measurements reveals that the efficiencies of both ATMS antenna sidelobes and cross-polarization are frequency dependent. From the ATMS pitchover maneuver data, it is found that the contributions of spacecraft radiation through the near-field sidelobes are significant and dominates the scan-angle-dependent features in the ATMS antenna temperatures. A theoretical model is developed for the conversion from antenna to sensor brightness temperatures, which incorporates the angular dependent terms derived from the pitchover maneuver data.**

***Index Terms*—Antenna pattern, Advanced Technology Microwave Sounder (ATMS), pitchover maneuver, Suomi National Polar-orbiting Partnership (NPP).**

I. Introduction

On October 28, 2011, the Suomi National Polar-orbiting Partnership (NPP) satellite was successfully launched into a circular near-polar afternoon-configured (1:30 P.M.) orbit at an altitude of 824 km above the Earth and an inclination angle of 98.7° to the equator. The Advanced Technology Microwave Sounder (ATMS) onboard the Suomi NPP satellite profiles atmospheric temperature and moisture in all-weather conditions and supports continuing advances in numerical weather prediction for improved short- to medium-range weather forecast skills.

ATMS calibration data, including raw radiometer counts, geolocation, telemetry, and housekeeping data, have been fully processed at the Suomi NPP Interface Data and Processing Segment since the instrument was turned on November 7, 2011. The ATMS antenna temperature data records (TDR) are now being distributed to user community from NOAA's Comprehensive Large Array-Data Stewardship Systems. Traditionally, the sensor brightness temperature data records (SDR) from satellite microwave sounding instruments are used in various applications. To compute the ATMS SDR from the TDR data, one must know the antenna properties such as the main beam efficiency, the spillover contributions from sidelobes and cross-polarization, and the accuracy of polarization angle alignment.

The conversion from TDR to SDR brightness temperatures for Advanced Microwave Sounding Unit-A (AMSU-A) and Humidity Sounding Unit (MHS) involves a radiometric calibration and a correction of the antenna sidelobe effects [1]. However, a strong scan-dependent bias exists in AMSU-A/MHS SDR data [2]–[5]. An asymmetric bias for AMSU-A window channels 1 and 2 was found by Weng *et al.* [6], who pointed out a twist of the antenna polarization angle as a possible root cause. This study aims at a full characterization of ATMS scan-angle-dependent biases from the ATMS pitchover maneuver data and presents the antenna theory of the cross-track scanning microwave radiometer.

II. Characteristics of ATMS Instrument

ATMS is a total power cross-track scanning microwave radiometer and has 22 channels, providing both temperature soundings from the surface to about 1 hPa (i.e., about 45 km) and humidity soundings from the surface to about 200 hPa (i.e., about 15 km). Table I provides selected channel characteristics for ATMS. Out of the 22 ATMS channels, 16 (channels 1–3, 5–15, 20, and 22) have the same frequencies as its predecessor AMSU-A/MHS. Three new channels are added: one for temperature sounding (i.e., ATMS channel 4) and two for humidity sounding (i.e., ATMS channels 19 and 21). The ATMS channels 16–18 (88.2 GHz, 165.5 GHz, 183.31 ± 7.0 GHz) are slightly different from MHS channels 16, 17, and 18 (89.0 GHz, 157.0 GHz, 190.31 GHz).

The ATMS calibration algorithms involve determining the blackbody brightness temperature and a temperature-dependent bias correction. Brightness temperatures of blackbody are measured by the embedded platinum resistance thermometer. The blackbody and cold-space radiation components are sampled four times in each calibration cycle and then averaged. These averaged values are further smoothed over several calibration cycles. The radiometer gain is calculated from the smoothed blackbody and cold-space radiation counts and is then used to estimate the Earth scene brightness temperature from a two-point linear calibration equation. The nonlinearity amplitude

Manuscript received May 29, 2012; revised September 4, 2012; accepted October 3, 2012. Date of publication November 26, 2012; date of current version February 20, 2013. The work of H. Yang and X. Zou was supported by the Chinese Ministry of Science and Technology under Project 2010CB951600. The views expressed in this publication are those of the authors and do not necessarily represent those of NOAA.

F. Weng is with the National Environmental Satellite, Data, and Information Service, National Oceanic and Atmospheric Administration, Washington, DC, USA (e-mail: Fuzhong.Weng@noaa.gov).

H. Yang is with the Department of Atmospheric and Oceanic Science, University of Maryland, College Park, MD 20742-2425 USA.

X. Zou is with the Department of Earth, Ocean and Atmospheric Sciences, Florida State University, Tallahassee, FL 32306-4520 USA.

Color versions of one or more of the figures in this paper are available online at http://ieeexplore.ieee.org.

Digital Object Identifier 10.1109/LGRS.2012.2223193

1545-598X/$31.00 © 2012 IEEE

TABLE I
ATMS SPECTRAL CHARACTERISTICS

Channel	Frequency (GHz)	WF (hPa)	NEΔT (K)	Beam width	Nadir FOV (km)
1	23.80	surface	0.90	5.2	74.78
2	31.40	surface	0.90	5.2	74.78
3	50.30	surface	1.20	2.2	31.64
4	51.76	surface	0.50	2.2	31.64
5	52.80	1000	0.75	2.2	31.64
6	53.596±0.115	700	0.75	2.2	31.64
7	54.40	400	0.75	2.2	31.64
8	54.94	270	0.75	2.2	31.64
9	55.50	180	0.75	2.2	31.64
10	57.29	90	0.75	2.2	31.64
11	57.29±0.217	50	1.20	2.2	31.64
12	57.29±0.322± 0.048	25	1.20	2.2	31.64
13	57.29±0.322 ± 0.022	10	1.50	2.2	31.64
14	57.29±0.322 ± 0.010	6	2.40	2.2	31.64
15	57.29±0.322± 0.0045	3	3.60	2.2	31.64
16	88.20	surface	0.50	2.2	31.64
17	165.50	1000	0.60	1.1	15.82
18	183.31±7.0	800	0.80	1.1	15.82
19	183.31±4.5	700	0.80	1.1	15.82
20	183.31±3.0	600	0.80	1.1	15.82
21	183.31±1.8	500	0.80	1.1	15.82
22	183.31±1.0	400	0.90	1.1	15.82

is estimated using the difference between the measured instrument temperature and that from two-point calibration. This implicit transfer function is applied to the Earth-scene counts for every scan cycle.

III. ATMS ANTENNA PATTERN MODEL

There are two receiving antennas on ATMS: one serving 15 channels below 60 GHz and the other for seven channels above 60 GHz. Both antennas consist of a plane reflector mounted on a scan axis at a 45° tilt angle. The scan axis is oriented in parallel with the along-track direction. Radiation is reflected from a direction perpendicular to the scan axis into a direction along the scan axis (i.e., a 90° reflection), resulting in a cross-track scan pattern. This reflected radiation is then focused by a stationary parabolic reflector onto a dichroic plate where the energy is either reflected to or passed through to a feedhorn (see Fig. 1) [7].

For a microwave antenna system, the radiative components from the Earth and other targets are collected through its main beam and the sidelobes. The magnitude of sidelobes depends on both frequency and antenna size. In general, the higher the frequency and the larger the antenna size, the narrower the main beam and the smaller the sidelobe effect. Fig. 2 shows the normalized ATMS antenna pattern distribution function at channel 1. The antenna pattern is shown in a decibel scale through normalizing the measured intensity in each direction by the sum of copolarized and cross-polarized radiation. Based on the normalized antenna pattern, the beamwidth, copolarized and cross-polarized beam efficiency for main and sidelobes could be computed. The main beam efficiency is computed at about 2.5 times half-power beamwidth. It is shown in Fig. 2 that the main beam efficiency is about −0.017 dB, whereas the sidelobe magnitude is less than −30 dB. Since the Suomi NPP satellite orbits an orbital altitude of 824 km, it can be roughly estimated that about 0.0002% to 0.01% of radiation from sidelobes can be

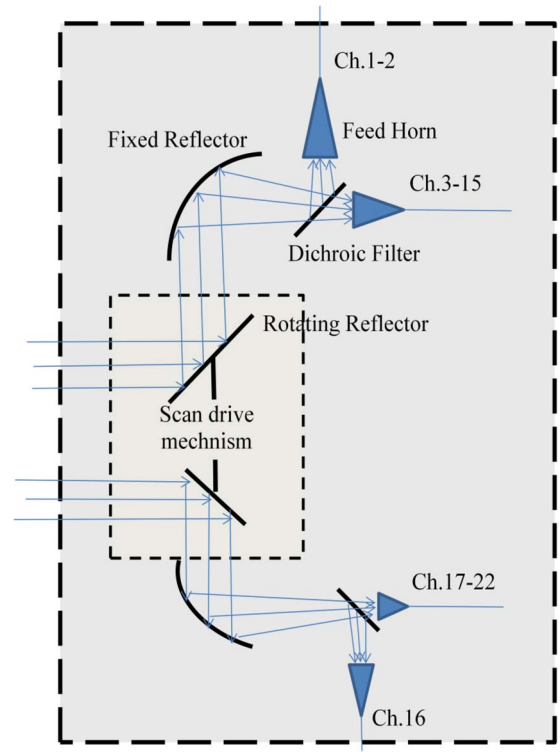

Fig. 1. Schematic of ATMS antenna subsystem (Chu, 2007).

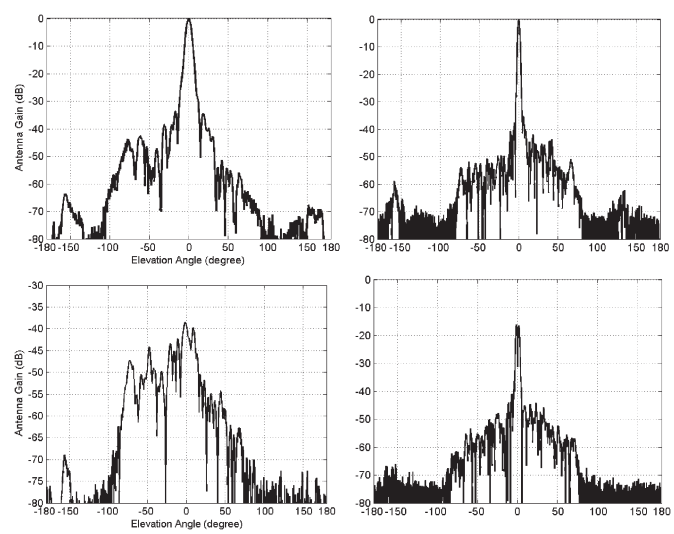

Fig. 2. ATMS normalized antenna pattern for channel 1 at (upper panels) copolarization and (lower panels) cross-polarization at three different scan angles: 52.7° (scan starting point, left panels), 0° (nadir point, middle panels), and −52.7° (scan ending point, right panels).

received from the 124° sector around the nadir that "sees" the Earth. By including not only the main beam efficiency of the Earth but also the sidelobe contributions from the Earth, cold space, and satellite platform, the satellite measured radiation is a result of radiation arrived at the front of antenna and convolved with the antenna pattern functions as follows:

$$T_a^p = \int_{\Omega_{me}} d\Omega\,(G^{pp}T_b^p + G^{qp}T_b^q) + \int_{\Omega_{se}} d\Omega\,(G^{pp}E_b^p + G^{qp}E_b^q) + \int_{\Omega_{sc}} d\Omega\,(G^{pp}C_b^p + G^{qp}C_b^q) + \int_{\Omega_{ss}} d\Omega\,(F^{pp}S_b^p + F^{qp}S_b^q) \quad (1)$$

where the superscripts p and q stand for either the v or h polarization state; G^{pp} and G^{qp} are the normalized antenna gain in the far-field (i.e., Earth and cold space) for copolarization and cross-polarization, respectively; F^{pp} and F^{qp} are the copolarization and cross-polarization antenna gain in the near-field (i.e., satellite platform); T_b is the brightness temperature of the Earth scene illuminated by the main beam; E_b, C_b, and S_b are the brightness temperatures of the Earth, cold space, and satellite platform seen by the sidelobes, respectively; Ω_{me} and Ω_{se} are the solid angles corresponding to the antenna main beam and sidelobes of the Earth, respectively; and Ω_{sc} and Ω_{ss} are the solid angles of the sidelobes seeing the cold space and satellite platform, respectively. The solid angle, i.e., Ω_{me}, corresponds to 2.5 times the main beamwidth $(\theta_{3\,\mathrm{dB}})$ that is calculated from a half-power width of the antenna pattern function, and its value is shown in Table I in degree. The first term in (1) is the Earth radiation entering into the receiver system through the main beam, which is determined by 2.5 times half-power beamwidth; the second term is the Earth radiation through the sidelobes that are out of the main beam but within the Earth view sector; the third term is the cold-space radiation through the sidelobes; and the fourth term is the radiation scattered and emitted from satellite platform to the receiver.

Assuming homogeneous brightness temperatures within relevant solid angles, the antenna temperature in (1) can be written as

$$T_a^p = \eta_{me}^{pp} T_b^p + \eta_{me}^{qp} T_b^q + \eta_{se}^{pp} E_b^p + \eta_{se}^{qp} E_b^q + \eta_{sc}^{pp} C_b^p + \eta_{sc}^{qp} C_b^q + \gamma_{ss}^{pp} S_b^p + \gamma_{ss}^{qp} S_b^q \quad (2)$$

where η_{me}^{pp}, η_{se}^{pp}, η_{sc}^{pp}, and γ_{ss}^{pp} are the copolarized antenna beam efficiencies and are defined as follows:

$$\eta_{me}^{pp} = \int_{\Omega_{me}} G^{pp} d\Omega \Big/ \int_{\Omega} (G^{pp} + G^{qp}) d\Omega$$
$$\eta_{se}^{pp} = \int_{\Omega_{ee}} G^{pp} d\Omega \Big/ \int_{\Omega} (G^{pp} + G^{qp}) d\Omega$$
$$\eta_{sc}^{pp} = \int_{\Omega_{ss}} G^{pp} d\Omega \Big/ \int_{\Omega} (G^{pp} + G^{qp}) d\Omega$$
$$\gamma_{ss}^{pp} = \int_{\Omega_{ss}} F^{pp} d\Omega \Big/ \int_{\Omega} (F^{pp} + F^{qp}) d\Omega.$$

The cross-polarized antenna beam efficiencies, i.e., η_{me}^{pq}, η_{se}^{pq}, η_{sc}^{pq}, and γ_{ss}^{pq}, have similar definitions except for replacing G^{pp} and F^{pp} in the numerators of the above equations by G^{pq} and F^{pq}.

For a normal scan of ATMS, η_{se}^{pp} is computed by integration of radiation intensity over -3-dB solid angle, η_{se}^{pp} is computed by integration of antenna radiation intensity between -3-dB angle and $\pm 62^\circ$ Earth boundary angle, and η_{sc}^{pp} is computed within the remaining angle range of the measured antenna pattern out of the Earth boundary. Since the near-field antenna pattern is not available, γ_{ss}^{pp} is approximately calculated using the far-field antenna pattern G^{pp}, which is to be denoted as η_{ss}^{pp}. The computed copolarized and cross-polarized main beam efficiency, as well as the sum of the three sidelobe beam efficiencies, are listed in Table II for 14 ATMS channels of typical frequencies.

TABLE II
BEAM EFFICIENCY VALUES AT TYPICAL CHANNELS OF ATMS INSTRUMENT

Frequency (GHz)	θ_{3dB} (degree)	η_{me}^{pp} (%)			η_{me}^{pq} (%)			$\eta_{se}^{pp}+\eta_{sc}^{pp}+\eta_{ss}^{pp}$ (%)		
		B1	B48	B96	B01	B48	B96	B01	B48	B96
23.8	5.2	95.5	95.3	95.9	0.84	0.73	0.81	3.66	3.97	3.29
31.4	5.2	97.0	96.4	96.8	0.64	0.65	0.64	2.36	2.95	2.56
50.3	2.2	96.2	95.6	96.3	1.01	1.05	0.90	2.79	3.35	2.80
51.8	2.2	96.2	95.7	96.6	0.95	0.94	0.70	2.85	3.36	2.70
52.8	2.2	96.2	95.8	96.1	0.87	0.91	0.98	2.93	3.29	2.92
53.6	2.2	96.3	95.9	96.2	0.88	0.94	1.04	2.82	3.16	2.76
54.4	2.2	96.5	96.1	96.6	0.87	0.86	0.82	2.63	3.04	2.58
54.9	2.2	96.6	96.1	96.2	0.90	0.90	1.13	2.50	3.00	2.67
55.5	2.2	96.7	96.2	96.6	0.90	0.88	0.86	2.40	2.92	2.54
57.3	2.2	97.3	97.1	97.2	0.92	0.91	0.93	1.78	1.99	1.87
88.2	2.2	90.9	91.3	91.7	4.71	4.65	4.54	4.39	4.05	3.76
166	1.1	86.2	83.9	86.6	3.71	3.40	5.18	10.09	12.7	8.22
183	1.1	86.0	87.4	89.3	4.03	2.25	1.85	9.97	10.35	8.85
183±7	1.1	86. 5	85.2	85.2	3.31	3.46	5.12	10.19	11.34	9.68

As the ATMS antenna scans across from nadir to its limb position, it receives signals from both the horizontal and vertical polarizations and obtains the so-called quasi-vertical (Qv) and quasi-horizontal (Qh) antenna temperature according to the following equations:

$$T_a^{Qv} = T_a^v \cos^2\theta + T_a^h \sin^2\theta \quad (3a)$$
$$T_a^{Qh} = T_a^v \sin^2\theta + T_a^h \cos^2\theta \quad (3b)$$

where θ is the scan angle, and T_a^v and T_a^h are the so-called SDR. T_a^{Qv} and T_a^{Qh} are referred to as TDR. For far-field radiation, we have $\eta^{vv} \simeq \eta^{hh}$, $\eta^{vh} \simeq \eta^{hv}$ (see Table II). Substituting (2) into (3) results in

$$T_a^{Qv} = \eta_{me}^{vv} T_b^{Qv} + \eta_{me}^{hv} T_b^{Qh} + \eta_{se}^{vv} E_b^{Qv} + \eta_{se}^{hv} E_b^{Qh} + \eta_{sc}^{vv} C_b^{Qv} + \eta_{sc}^{hv} C_b^{Qh} + S_a^{Qv} \quad (4a)$$
$$T_a^{Qh} = \eta_{me}^{hh} T_b^{Qh} + \eta_{me}^{vh} T_b^{Qv} + \eta_{se}^{hh} E_b^{Qh} + \eta_{se}^{vh} E_b^{Qv} + \eta_{sc}^{vv} C_b^{Qv} + \eta_{sc}^{hv} C_b^{Qh} + S_a^{Qh} \quad (4b)$$

where (T_b^{Qv}, T_b^{Qh}) are the radiation contributions from the Earth's main beam; (E_b^{Qv}, E_b^{Qh}) and (C_b^{Qv}, C_b^{Qh}) are the sidelobe contributions from the Earth and cold space, respectively; and (S_a^{Qv}, S_a^{Qh}) represents the contributions from the near-field radiation from spacecraft.

The sensor brightness temperatures of the Earth's main beam (T_b^v, T_b^h), Earth's sidelobes (E_b^v, E_b^h), cold-space sidelobes (C_b^v, C_b^h), and the near-field radiation contributions from spacecraft (S_b^v, S_b^h) can be expressed as follows:

$$A^{Qv} = A^v \cos^2\theta + A^h \sin^2\theta \quad (5a)$$
$$A^{Qh} = A^v \sin^2\theta + A^h \cos^2\theta \quad (5b)$$
$$S_a^{Qh} = \left(\gamma_{ss}^{vv} S_b^v + \gamma_{ss}^{hv} S_b^h\right) \sin^2\theta + \left(\gamma_{ss}^{hh} S_b^h + \gamma_{ss}^{vh} S_b^v\right) \cos^2\theta \quad (5c)$$
$$S_a^{Qh} = \left(\gamma_{ss}^{vv} S_b^v + \gamma_{ss}^{hv} S_b^h\right) \sin^2\theta + \left(\gamma_{ss}^{hh} S_b^h + \gamma_{ss}^{vh} S_b^v\right) \cos^2\theta \quad (5d)$$

where A in (5a) and (5b) stands for T_b, E_b, or C_b. Therefore, for a cross-track scanning system, the conversion from the antenna to sensor brightness temperatures requires an accurate characterization of all of the antenna main beam and sidelobe efficiencies, the Earth radiation from the main beam, and the radiation from the spacecraft.

In (4), the cold-space radiation can be estimated assuming a constant cosmic temperature at 2.73 K. However, the radiation components for the Earth view from the sidelobes are largely

unknown. In addition, the radiation from the spacecraft within the near-field sidelobes is not quantified in normal satellite operations. Based on the computed sidelobe beam efficiency values listed in Table II, we can reasonably assume that the sidelobe contributions to the total received radiation are small and can be ignored. Therefore, (4) can be written as

$$T_a^{Qv} = \eta_{me}^{vv} T_b^{Qv} + \eta_{me}^{hv} T_b^{Qh} + S_a^{Qv} \tag{6a}$$
$$T_a^{Qh} = \eta_{me}^{hh} T_b^{Qh} + \eta_{me}^{vh} T_b^{Qv} + S_a^{Qh}. \tag{6b}$$

In general, the conversion from the antenna temperature at a single polarization, i.e., T_a^{Qv} or T_a^{Qh}, to the sensor brightness temperatures, i.e., T_b^{Qv} and/or T_b^{Qh}, using (6) is not unique. Two simplifications can be considered. For an antenna system that has a zero cross-polarization efficiency ($\eta_{me}^{hv} = \eta_{me}^{vh} = 0$), (6) is simplified into

$$T_a^{Qv} = \eta_{me}^{vv} T_b^{Qv} + S_a^{Qv}, \qquad T_a^{Qh} = \eta_{me}^{hh} T_b^{Qh} + S_a^{Qh}. \tag{7}$$

If the natural Earth radiation has no polarization ($T_b^{Qv} = T_b^{Qh}$), (6) becomes

$$\begin{aligned} T_a^{Qv} &= \left(\eta_{me}^{vv} + \eta_{me}^{hv}\right) T_b^{Qv} + S_a^{Qv} \\ T_a^{Qh} &= \left(\eta_{me}^{hh} + \eta_{me}^{vh}\right) T_b^{Qv} + S_a^{Qh}. \end{aligned} \tag{8}$$

The conversion from TDR to SDR becomes unique in these two cases if the radiation terms related to spacecraft, i.e., S_a^{Qv} and S_a^{Qh}, can be estimated. In Section IV, the pitchover maneuver observations of ATMS are used for estimating the last term on the right-hand side of (7) and (8).

IV. Analysis of ATMS Pitchover Maneuver Data

On February 20, 2012, the Suomi NPP satellite made its pitchover maneuver. The spacecraft is completely pitched off the Earth to enable ATMS to acquire full scans of deep space. Fig. 3 shows the orbit on which the pitchover maneuver was performed. During a 43-minute period of ATMS pitch maneuver, the antenna is ramped up at a linear rate for the first 11 minutes, held to scan the cold space for about 22 minutes, and then ramped down at a linear rate to its normal Earth scanning position in the final 10 minutes. During the 22-minute pitchover period, ATMS continually scanned cold space across its 96 field of views (FOVs). Since the Earth's disk lies outside of the main beam and the cold-space radiation within the antenna's sidelobes is very uniform, any additional radiation introduced by obstacles on the spacecraft could be observed. These observations are used here for evaluating the scan angle dependence of the antenna temperature model developed in Sections III and IV. The maneuver will also allow us to establish the baseline radiometer output (i.e., counts) from the sidelobe effect of cold space and spacecraft.

When ATMS performs a space scan during its pitchover maneuver period, the cold-space radiation is uniform and unpolarized, the copolarization and cross-polarization terms in (4a) and (4b) can be merged into one single term, i.e.,

$$\begin{aligned} T_a^{Qv} &= \eta_{me}^{vv} C_b + \eta_{me}^{hv} C_b + \eta_{se}^{vv} E_b^{Qv} + \eta_{se}^{hv} E_b^{Qh} \\ &\quad + \eta_{sc}^{vv} C_b + \eta_{sc}^{hv} C_b + S_a^{Qv} \end{aligned} \tag{9a}$$
$$\begin{aligned} T_a^{Qh} &= \eta_{me}^{hh} C_b + \eta_{me}^{vh} C_b + \eta_{se}^{hh} E_b^{Qh} + \eta_{se}^{vh} E_b^{Qv} \\ &\quad + \eta_{sc}^{hh} C_b + \eta_{sc}^{vh} C_b + S_a^{Qh}. \end{aligned} \tag{9b}$$

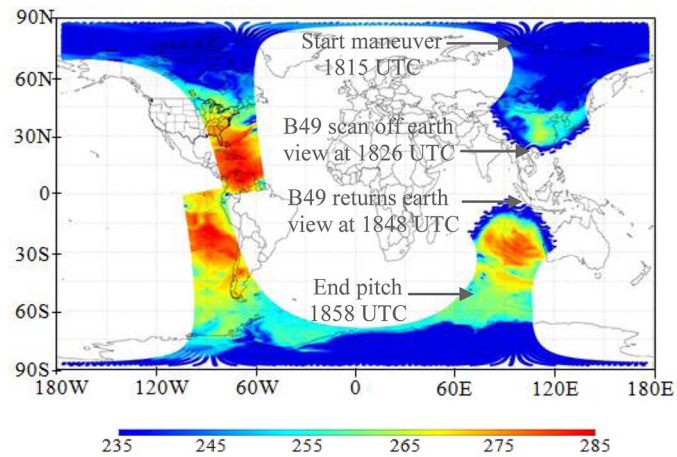

Fig. 3. ATMS pitchover maneuver locations and time zone.

By neglecting the sidelobes of the Earth, the space scan antenna temperature can be written as

$$T_a^{Qv} = \left(\eta_m^{vv} + \eta_m^{hv}\right) C_b + S_a^{Qv} \tag{10a}$$
$$T_a^{Qh} = \left(\eta_m^{hh} + \eta_m^{vh}\right) C_b + S_a^{Qh} \tag{10b}$$

where $\eta_m = \eta_{me} + \eta_{sc}$ represents the beam efficiency contribution from both the main beam and the sidelobes that view the space radiation.

Contributions of the radiation from the spacecraft can be quantified if the radiation from the spacecraft is unpolarized (i.e., $S_b^v = S_b^h \equiv S_b$) and the near-field sidelobe efficiency is different between two copolarizations (i.e., $\gamma_{ss}^{hh} > \gamma_{ss}^{vv}$), then (5c) and (5d) can be simplified into

$$\begin{aligned} S_a^{Qv} &= \gamma_{ss}^{vv} S_b \cos^2\theta + \gamma_{ss}^{hh} S_b \sin^2\theta \\ S_a^{Qh} &= \gamma_{ss}^{vv} S_b \sin^2\theta + \gamma_{ss}^{hh} S_b \cos^2\theta. \end{aligned}$$

As a result, (10) becomes

$$\begin{aligned} T_a^{Qv} &= \left(\eta_m^{vv} + \eta_m^{hv}\right) C_b + \gamma_{ss}^{vv} S_b + \Delta\gamma S_b \sin^2\theta \\ &\equiv \left(\eta_m^{vv} + \eta_m^{hv}\right) C_b + \beta_0^v + \beta_1^v \sin^2\theta \end{aligned} \tag{11a}$$
$$\begin{aligned} T_a^{Qh} &= \left(\eta_m^{hh} + \eta_m^{vh}\right) C_b + \gamma_{ss}^{hh} S_b + \Delta\gamma S_b \cos^2\theta \\ &\equiv \left(\eta_m^{hh} + \eta_m^{vh}\right) C_b + \beta_0^h + \beta_1^h \cos^2\theta \end{aligned} \tag{11b}$$

where $\Delta\gamma = \gamma_{ss}^{hh} - \gamma_{ss}^{vv}$.

If the spacecraft radiation is polarized and the near-field sidelobe efficiency is the same for both copolarizations (i.e., $\gamma_{ss}^{hh} = \gamma_{ss}^{vv}$), then (10) becomes

$$\begin{aligned} T_a^{Qv} &= \left(\eta_m^{vv} + \eta_m^{hv}\right) C_b + \gamma_{ss}^{vv} S_b^v + \gamma_{ss}^{vv} \left(S_b^h - S_b^v\right) \sin^2\theta \\ &\equiv \left(\eta_m^{vv} + \eta_m^{hv}\right) C_b + \beta_0^v + \beta_1^v \sin^2\theta \end{aligned} \tag{12a}$$
$$\begin{aligned} T_a^{Qh} &= \left(\eta_m^{hh} + \eta_m^{vh}\right) C_b + \gamma_{ss}^{hh} S_b^h + \gamma_{ss}^{hh} \left(S_b^h - S_b^v\right) \cos^2\theta \\ &\equiv \left(\eta_m^{hh} + \eta_m^{vh}\right) C_b + \beta_0^h + \beta_1^h \cos^2\theta. \end{aligned} \tag{12b}$$

From (11) and (12), it is concluded that the antenna temperature from a space view is composed of the far-field deep space radiation from the main beam and the near-field satellite platform radiation. The space scan antenna temperature is scan angle dependent, which is different for quasi-vertical and quasi-horizontal polarization. The antenna temperature along a scan-line for a quasi-vertical polarization curves up (i.e., a smiling feature) and that for a quasi-horizontal curves down (i.e., a frown feature) if the antenna side efficiency for the copolarizations meets the condition of $\gamma_{ss}^{hh} > \gamma_{ss}^{vv}$ or if the radiation from spacecraft satisfies the condition of $S_b^h - S_b^v > 0$.

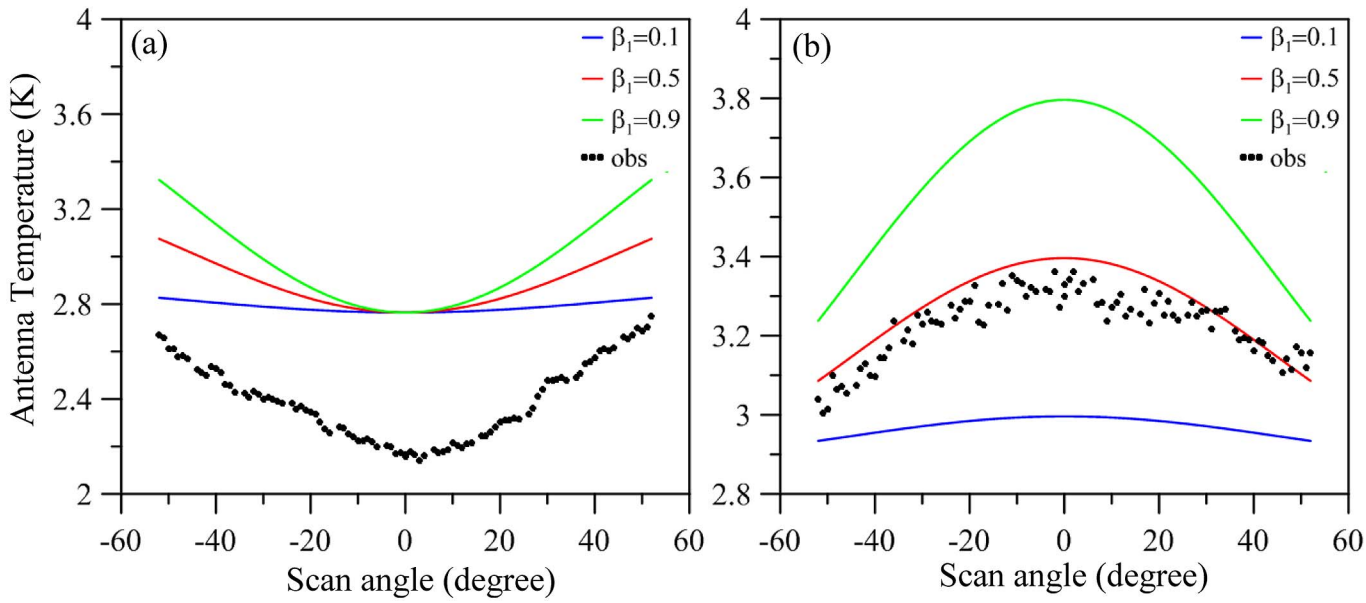

Fig. 4. Variation of the model-simulated antenna temperature with respect to scan angle (curves) for a typical ATMS (a) quasi-vertical polarization channel (channel 1) and (b) quasi-horizontal polarization channel (channel 4) for three specified values of β_1. The ATMS measured antenna temperatures for the same channels during pitchover maneuver are shown in black.

Fig. 4 shows the variation of the simulated antenna temperature with respect to scan angle for a typical ATMS quasi-vertical polarization channel (channel 1) and a typical quasi-horizontal polarization channel (channel 4) for three specified values of β_1. The ATMS measured antenna temperatures for the same channels during pitchover maneuver are also shown in Fig. 4. The larger the value of β_1, the more significant the satellite platform effect; the model-simulated antenna temperature varies more rapidly with scan angle. The scan angle dependence features of model-simulated antenna temperature for both quasi-vertical and quasi-horizontal polarization are consistent with maneuver measurements. The observed and model-simulated antenna temperatures have either a minimum [see Fig. 4(a), quasi-vertical channel] or a maximum [see Fig. 4(b), quasi-horizontal] at nadir. It is noticed that the observations at channel 1 are much lower than the theoretical cold-space brightness temperature. This is probably due to the residual bias of radiometric calibration in the ground processing system. For example, the ATMS calibration equation is directly based on brightness temperature instead of radiance, which is only valid in low frequency. In addition, the cold-space calibration temperature is determined during a prelaunch period and could have a systematic bias. Since the last term in (8) largely determines the scan angle dependence of the TDR when ATMS scans through the cold space, the scan-angle-dependent pattern from pitchover maneuver data shown in Fig. 4 could be used to resolve the near-field terms in (4) when ATMS scans the Earth.

V. Summary

Quantifying the scan-angle-dependent brightness temperature biases introduced by antenna sidelobes is important for ATMS calibration. The pitchover maneuver of the Suomi NPP satellite enables ATMS to acquire full scans of deep space, providing a unique opportunity to study the scan bias characteristics. ATMS antenna temperature measurements during its pitchover period exhibits a distinct scan-angle-dependent feature but different for quasi-vertical and horizontal polarization channels. Analysis of far-field antenna pattern for all ATMS 22 channels shows that for both space and Earth scans, the cross-polarization term as well as near-field reflection and emission from satellite platform have some contributions to ATMS measurements. A theoretical model is established to explain the scan-angle-dependent feature of ATMS measurement bias, with model parameters derived from the pitchover maneuver data. It is anticipated that the scan-angle-dependent feature of measurement bias can be significantly removed by applying this model to the Earth scene simulation of ATMS data.

Acknowledgment

The authors would like to thank Dr. X. Wang and Dr. N. Sun for preparing the ATMS data and plots.

References

[1] T. Mo, "AMSU-A antenna pattern corrections," *IEEE Trans. Geosci. Remote Sens.*, vol. 37, no. 1, pp. 103–112, Jan. 1999.
[2] A. Stogryn, "Estimates of brightness temperatures from scanning radiometer data," *IEEE Trans. Antennas Propag.*, vol. AP-26, no. 5, pp. 720–726, Sep. 1978.
[3] B. A. Harris and G. Kelly, "A satellite radiance-bias correction scheme for data assimilation," *Q. J. R. Meteorol. Soc.*, vol. 127, no. 574, pp. 1453–1468, Apr. 2001.
[4] S. A. Buehler and V. O. John, "A simple method to relate microwave radiances to upper tropospheric humidity," *J. Geophys. Res.*, vol. 110, pp. D02110-1–D02110-11, Jan. 2005.
[5] L. Guan, X. Zou, F. Weng, and G. Li, "Assessments of FY3A microwave humidity sounder measurements using NOAA18 microwave humidity sounder," *J. Geophys. Res.*, vol. 116, pp. D10106-1–D10106-17, May 2011.
[6] F. Weng, L. Zhao, R. R. Ferraro, G. Poe, X. Li, and N. Grody, "Advanced microwave sounding unit cloud and precipitation algorithms," *Radio Sci.*, vol. 38, no. 33, pp. 8068–8081, Jun. 2003.
[7] R. Chu, Joint Polar Satellite System (JPSS) Advanced Technology Microwave Sounder (ATMS) SDR Radiometric Calibration Algorithm Theoretical Basic Document (ATBD), p. 17, 2007. [Online]. Available: http://www.star.nesdis.noaa.gov/jpss/ATBD.php#S120122